

5-1-2019

A thin film flow of nanofluid comprising carbon nanotubes influenced by Cattaneo-Christov heat flux and entropy generation

Dianchen Lu
Jiangsu University

Muhammad Ramzan
Bahria University

Mutaz Mohammad
Zayed University, mutaz.mohammad@zu.ac.ae

Fares Howari
Zayed University

Jae Dong Chung
Sejong University

Follow this and additional works at: <https://zuscholars.zu.ac.ae/works>



Part of the [Life Sciences Commons](#)



Recommended Citation

Lu, Dianchen; Ramzan, Muhammad; Mohammad, Mutaz; Howari, Fares; and Chung, Jae Dong, "A thin film flow of nanofluid comprising carbon nanotubes influenced by Cattaneo-Christov heat flux and entropy generation" (2019). *All Works*. 300.
<https://zuscholars.zu.ac.ae/works/300>

This Article is brought to you for free and open access by ZU Scholars. It has been accepted for inclusion in All Works by an authorized administrator of ZU Scholars. For more information, please contact scholars@zu.ac.ae.

Article

A Thin Film Flow of Nanofluid Comprising Carbon Nanotubes Influenced by Cattaneo-Christov Heat Flux and Entropy Generation

Dianchen Lu ¹, Muhammad Ramzan ^{2,3,*}, Mutaz Mohammad ^{4,*}, Fares Howari ⁵ and Jae Dong Chung ³

¹ Department of Mathematics, Faculty of Science, Jiangsu University, Zhenjiang 212013, China; dclu@ujs.edu.cn

² Department of Computer Science, Bahria University, 44000 Islamabad, Pakistan

³ Department of Mechanical Engineering, Sejong University, Seoul 143-747, Korea; jdchung@sejong.edu

⁴ Department of Mathematics and Statistics, College of Natural and Health Sciences, Zayed University, 144543 Abu Dhabi, UAE

⁵ College of Natural and Health Sciences, Zayed University, 144543 Abu Dhabi, UAE; fares.howari@zu.ac.ae

* Correspondence: mramzan@bahria.edu.pk (M.R.); mutaz.mohammad@zu.ac.ae (M.M.);

Tel.: +92-30-05-122-700 (M.R.); +971-2-599-3496 (M.M.)

Received: 30 March 2019; Accepted: 24 April 2019; Published: 1 May 2019



Abstract: This study aims to scrutinize the thin film flow of a nanofluid comprising of carbon nanotubes (CNTs), single and multi-walled i.e., (SWCNTs and MWCNTs), with Cattaneo-Christov heat flux and entropy generation. The time-dependent flow is supported by thermal radiation, variable source/sink, and magneto hydrodynamics past a linearly stretched surface. The obtained system of equations is addressed by the numerical approach *bvp4c* of the MATLAB software. The presented results are validated by comparing them to an already conducted study and an excellent synchronization in both results is achieved. The repercussions of the arising parameters on the involved profiles are portrayed via graphical illustrations and numerically erected tables. It is seen that the axial velocity decreases as the value of film thickness parameter increases. It is further noticed that for both types of CNTs, the velocity and temperature distributions increase as the solid volume fraction escalates.

Keywords: thin liquid film flow; carbon nanotubes; Cattaneo-Christov heat flux; variable heat source/sink; entropy generation

1. Introduction

The flow and heat transfer phenomenon in thin fluid film past stretched surfaces has promising applications including continuous casting, extrusion of plastic sheets, drawing of polymer surfaces, foodstuff processing, annealing and tinning of copper wires, and cooling of metallic plates [1]. The maintenance of the extrudes' surface is vital in the extrusion process smooth surface with minimum friction and enough strength is necessary for the coating procedure. Additionally, all this highly rely on the flow and heat transfer properties of the thin film over stretched surfaces. Because of this, the analysis in such cases is quite essential. Wang's [2] pioneering work by deliberating the hydrodynamics of time-dependent thin fluid film flow past a stretching sheet invited researchers to work in this attractive industry-oriented theme. Andersson et al. [3] further developed Wang's idea for heat transfer analysis. This case is further presented in a more generalized form by Chung and Andersson [4]. The solution to the same problem is discussed analytically by Wang [5]. The thin film flow is later analyzed

in various scenarios like magnetic impact [6,7], thermo-capillary impacts [8], and non-Newtonian fluids [9–12].

The above-mentioned studies on thin liquid films are limited to Newtonian and non-Newtonian fluids in the absence of nanofluids. In recent years, the subject of nanofluids, owing to their amazing characteristic of high thermal conductivity, has gained much attention of researchers and scientists. The seminal work by Choi and Eastman [13] introducing “nanofluids” has revolutionized the heat transfer processes. A nanofluid is an amalgamation of the solid metallic particles called “Nanoparticles” with a size of 1–100 nm and ordinary liquids. Nanofluids are the finest coolants with amazing applications including microelectronics, optical manufacturing and transportation [14]. There are studies that emphasize the thin film liquid flow of nanofluids. Lin et al. [15] numerically scrutinized the thin film Pseudo-plastic nano liquid flow with the impact of internal heat generation by utilizing R–K scheme and Newton’s method. Later, Lin et al. [16] extended this study to the impacts of viscous dissipation and temperature reliant thermal conductivity. The nano-liquid thin film flow comprising graphene nanoparticles under the influence of aligned magnetic effect is discussed by Sandeep [17]. Zhang et al. [18] studied the Oldroyd-B nanofluid thin film flow analytically with two types of nanoparticles, i.e., silver and copper and found that nanofluid containing silver nanoparticles has a better thermal conductivity in comparison to the copper nanoparticles. Zhang et al. [19] also deliberated the power law nano liquid thin film flow with the slip using the differential transform method. The problem of nanofluid thin films flowing past an elastic stretched sheet is solved using the least square method (LSM) by Fakour et al. [20]. Ishaq et al. [21] deliberated the analytical solution of Powell-Eyring nano liquid thin film flow with thermal radiation past a permeable stretched surface. The flow of Darcy-Forchheimer nanofluid thin film comprising SWCNTs past an unsteady stretched surface is studied by Nasir et al. [22].

There are numerous applications of heat transfer in industrial and engineering processes. These include cooling towers, fuel cells, microelectronics, and nuclear reactors. The fundamental essence in all these processes is that the value of thermal conductivity is presumed to be a constant. However, this value varies with temperature and other factors. Pal [23] and Vajravelu et al. [24] observed that the thermal conductivity varies linearly as the temperature is altered from 0° to 400° F. Initially, the Fourier law of heat conduction has been used in the modeling of heat transfer applications but the system encounters an initial disturbance due to the “parabolic energy equation” which is referred to as “paradox in heat conduction”. This shortcoming in the Fourier’s model was addressed by Cattaneo [25] who introduced the thermal relaxation time in the Fourier law of heat conduction. Cattaneo’s act helped to represent the temperature profile via the hyperbolic energy equation and heat transport propagation using thermal waves with a controlled speed. This heat transport mechanism is employed in diverse practical scenarios, ranging from nano-liquid flow models to skin burn injury models [26]. Moreover, several materials possess a large thermal relaxation time, such as biological tissues having a relaxation time of 91–100 s and sand of 21 s. To uphold the material invariant formulation, Christov altered the Maxwell-Cattaneo model by swapping the time derivative with Oldroyd’s upper convected derivative. This improved version is nowadays being termed as the Cattaneo-Christov (C-C) heat flux model. Later, Han et al. [27] introduced an analytical solution for the viscoelastic material including the velocity slip boundary along with the C-C heat flux. Mustafa [28] analyzed the rotating flow of the Maxwell fluid with an upper convected derivative and C-C heat flux over a linearly stretched surface using both the analytical and numerical methods. A similar case was examined by Khan et al. [29] considering an exponentially stretched surface. The squeezed flow of the C-C heat flux with CNTs between two parallel disks is studied by Lu et al. [30]. Ramzan et al. [31] studied the flow of the Williamson fluid flow numerically with C-C heat flux associated with the convective boundary condition and homogeneous-heterogeneous reactions. The flow of the magnetohydrodynamics (MHD) second-grade fluid over a stretched cylinder with C-C heat flux is discussed by Alamri et al. [32]. Ramzan et al. [33,34] deliberated the Maxwell and third-grade fluid flows with homogeneous-heterogeneous reactions and C-C heat flux. The flow of

aqueous based nanotubes with homogeneous-heterogeneous reactions past a Darcy-Forchheimer three-dimensional flow is studied by Alshomrani and Ullah [35]. Saleem et al. [36] discussed the squeezing three-dimensional nanofluid flow comprising of nanotubes in a Darcy-Forchheimer medium with thermal radiation and heat generation/absorption. There are numerous explorations that discuss on the flow of nanofluid amalgamated with carbon nanotubes in various scenarios but there are fewer that address the thin film flow. Some more explorations focusing on carbon nanotube or nanofluid flow may be found in References [37–40] and many therein.

The literature review reveals that the flow of a thin film with the Newtonian/non-Newtonian fluids is scarce in the literature and this subject gets even narrower if we talk about the thin film flows of nanofluids. Very few explorations are available that discuss the thin film flows of nanofluid-comprising nanotubes. Keeping in mind the importance of hydrodynamic flows, the idea of nanoliquid thin films in comparatively new and fewer explorations are available in the literature (see Table 1). This presented model is solved numerically and will present an estimated solution. The other limitation of the flow is that it is discussed in 2D and can be extended to 3D with some more novel effects like homogeneous-heterogeneous reactions, etc. The model presented here is an amalgamation of C-C heat flux and entropy generation in the thin film flows of the nanofluids comprising of both types of nanotubes (SWCNTs/MWCNTs) and has not yet been discussed in the literature. The numerical solution of the problem is achieved. A comparison with an already established result in the limiting case is also given and an excellent agreement between both is found. This corroborates our presented results. The graphical illustrations and numerically calculated values of the physical parameters are also added to the problem.

Table 1. The studies on nanoliquid film flow.

Authors	Nanofluid Models	Film Thickness	Nanotubes SWCNTs/MWCNTs	C-C Heat Flux
Lin et al. [15]	Tiwari and Das	√	×	×
Sandeep [17]	Tiwari and Das	√	×	×
Nasir et al. [22]	Tiwari and Das	√	SWCNTs	×
Narayana and Sibanda [41]	Tiwari and Das	√	×	×
Xu et al. [42]	Tiwari and Das	√	×	×
Qasim et al. [43]	Buongiorno's	√	×	×
Present	Tiwari and Das	√	√	√

(√) means effect is present and (×) means effect is absent.

2. Mathematical Modeling

Let us assume a thin film flow of a nanoliquid flow comprising CNTs past a time dependent linearly stretched surface. The elastic sheet emerges from a slender slit at the Cartesian coordinate system's origin (Figure 1). The surface moves along the x -axis ($y = 0$) with a velocity $u_w(x, t) = \frac{bx}{(1-\alpha t)}$, with b and a being the constants in the y -direction and temperature $T_w(x, y)$. The stream function ξ is considered such that $u = \xi_y$, and $v = -\xi_x$.

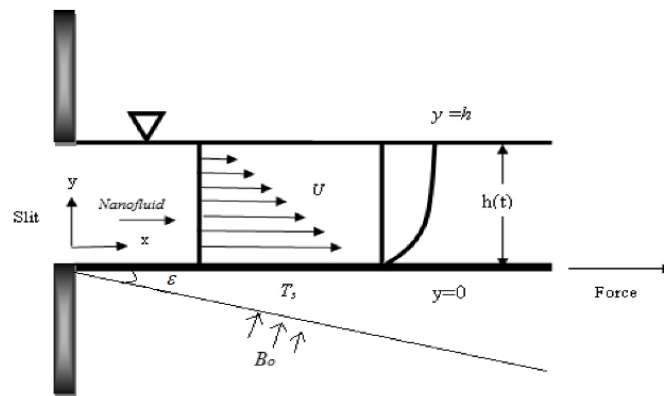


Figure 1. The flow geometry of the model.

The thin film is of width $h(x, y)$. The flow is laminar and incompressible. A magnetic field $B(x, t) = B_0(1 - at)^{-\frac{1}{2}}$, is employed normal to the extended surface. The governing unsteady conservation equations [17] under the aforementioned assumptions are appended as follows:

$$\frac{\partial^2 \xi}{\partial x \partial y} - \frac{\partial^2 \xi}{\partial y \partial x} = 0 \tag{1}$$

$$\frac{\partial^2 \xi}{\partial t \partial y} - \frac{\partial \xi}{\partial y} \frac{\partial^2 \xi}{\partial x \partial y} - \frac{\partial \xi}{\partial x} \frac{\partial^2 \xi}{\partial y^2} = v_{nf} \frac{\partial^3 \xi}{\partial y^3} + \frac{\sigma_{nf}}{\rho_{nf}} B^2(t) \frac{\partial \xi}{\partial y} \cos^2 \epsilon, \tag{2}$$

$$(\rho C_p)_{nf} \left(\frac{\partial T}{\partial t} + \frac{\partial \xi}{\partial y} \frac{\partial T}{\partial x} - \frac{\partial \xi}{\partial x} \frac{\partial T}{\partial y} \right) + \lambda_2 \Omega_2 = \left(k_{nf} + \frac{16 T_\infty^3 \sigma^*}{3 k^*} \right) \frac{\partial^2 T}{\partial y^2} + q''' \tag{3}$$

With the following corresponding boundary conditions

$$\begin{aligned} -\xi_x = 0, \xi_y = u_w, T = T_s, \quad \text{at } y = 0, \\ \xi_{yy} = 0, -\xi_x = h_t, T = 0, \quad \text{as } y = h(t). \end{aligned} \tag{4}$$

The Cattaneo-Christov term is defined as

$$\begin{aligned} \Omega_2 = \frac{\partial^2 T}{\partial t^2} + \frac{\partial u}{\partial t} \frac{\partial T}{\partial x} + 2 \frac{\partial \xi}{\partial y} \frac{\partial^2 T}{\partial t \partial x} - 2 \frac{\partial \xi}{\partial x} \frac{\partial^2 T}{\partial t \partial y} + \frac{\partial v}{\partial t} \frac{\partial T}{\partial y} + \frac{\partial \xi}{\partial y} \frac{\partial^2 \xi}{\partial x \partial y} \frac{\partial T}{\partial x} + \frac{\partial \xi}{\partial x} \frac{\partial^2 \xi}{\partial y \partial x} \frac{\partial T}{\partial y} \\ + \left(\frac{\partial \xi}{\partial y} \right)^2 \frac{\partial^2 T}{\partial x^2} + \left(\frac{\partial \xi}{\partial x} \right)^2 \frac{\partial^2 T}{\partial y^2} - 2 \frac{\partial \xi}{\partial y} \frac{\partial \xi}{\partial x} \frac{\partial^2 T}{\partial x \partial y} - \frac{\partial \xi}{\partial y} \frac{\partial^2 \xi}{\partial x^2} \frac{\partial T}{\partial y} - \frac{\partial \xi}{\partial x} \frac{\partial^2 \xi}{\partial y^2} \frac{\partial T}{\partial x} \end{aligned} \tag{5}$$

The heat source/sink “ q''' ” is represented by

$$q''' = \frac{k_f u_w (T_s - T_0)}{x v_f} \left(A^* f' + B^* \frac{(T - T_0)}{(T_s - T_0)} \right) \tag{6}$$

The thermophysical attributes (specific heat C_p , density ρ and thermal conductivity k) of the base fluid (H_2O) and carbon nanotubes (SWCNTs/MWCNTs) are appended in Table 2.

Table 2. The thermophysical physiognomies of the fluid and CNTs [30].

Physical Characteristics	Conventional Fluid	Nano Particles	
–	H ₂ O	SWCNTs	MWCNTs
C_p (J/kg K)	4179	425	796
ρ (kg/m ³)	997	2600	1600
k (W/mK)	0.613	6600	3000

The hypothetical relations are characterized as follows:

$$\mu_{nf} = \frac{\mu_f}{(1 - \phi)^{2.5}}, \nu_{nf} = \frac{\nu_{nf}}{\rho_{nf}}, \tag{7}$$

$$\rho_{nf} = (1 - \phi)\rho_f + \phi\rho_{CNT}, \alpha_{nf} = \frac{k_{nf}}{\rho_{nf}(c_p)_{nf}} \tag{8}$$

$$\frac{\sigma_{nf}}{\sigma_f} = 1 + \frac{3\sigma\phi - 3\phi}{\sigma + 2 - \sigma\phi + \phi}, \sigma = \frac{\sigma_{CNT}}{\sigma_f}, \tag{9}$$

$$\frac{k_{nf}}{k_f} = \frac{(1 - \phi) + 2\phi \frac{k_{CNT}}{k_{CNT} - k_f} \ln\left(\frac{k_{CNT} + k_f}{2k_f}\right)}{(1 - \phi) + 2\phi \frac{k_f}{k_{CNT} - k_f} \ln\left(\frac{k_{CNT} + k_f}{2k_f}\right)} \tag{10}$$

Using the similarity transformations

$$\eta = \frac{1}{\beta} \left(\frac{b}{\nu_f(1-at)} \right)^{\frac{1}{2}} y, \Psi = \beta \left(\frac{b\nu_f}{(1-at)} \right)^{\frac{1}{2}} x f(\eta), \theta = \frac{T - T_0}{T_s - T_0} \tag{11}$$

$$T = T_0 - T_r \left(\frac{bx^2}{2\nu_f} \right) (1 - at)^{-1.5} \theta(\eta),$$

The requirement of Equation (1) is fulfilled undoubtedly and Equations (2) and (3) yield

$$f''' + (1 - \phi)^{2.5} (1 - \phi + \phi \frac{\rho_{CNT}}{\rho_f}) \lambda \left\{ f f'' - f'^2 - S \left(f' + \frac{1}{2} \eta f'' \right) \right\} - (1 - \phi)^{2.5} \frac{\sigma_{nf}}{\sigma_f} M f' \cos^2 \varepsilon = 0 \tag{12}$$

$$\frac{\left(\frac{k_{nf}}{k_f} + \frac{4}{3} R \right)}{Pr \left[1 - \phi + \phi \frac{(\rho c_p)_{CNT}}{(\rho c_p)_f} \right]} \theta'' - \lambda \left[2f'\theta - f\theta' + \frac{S}{2} (3\theta + \eta\theta') \right] + \frac{1}{Pr \left[1 - \phi + \phi \frac{(\rho c_p)_{CNT}}{(\rho c_p)_f} \right]} (A^* f' + B^* \theta) \tag{13}$$

$$+ \gamma \left\{ \begin{aligned} & -\frac{15}{2} S^2 \theta - \frac{7}{2} S^2 \eta \theta' - \frac{1}{4} S^2 \eta^2 \theta'' - 8Sf'\theta - \eta Sf''\theta - \frac{3}{2} \eta Sf'\theta' \\ & + \frac{9}{2} Sf'\theta' + S\eta f\theta'' - 4f'^2\theta + 3ff'\theta' - f'^2\theta'' + 2ff''\theta \end{aligned} \right\} = 0,$$

Additionally, the boundary conditions of Equation (4) become

$$f(0) = 0, f'(0) = 1, \theta(0) = 1, f(1) = \frac{S}{2}, f''(1) = 0, \theta'(1) = 0 \tag{14}$$

The values of various non-dimensional parameters are defined as follows:

$$Pr = \frac{\nu_f}{\alpha_f}, S = \frac{\alpha}{b}, R = \frac{4\sigma^* T_0^3}{k^* k_f}, M = \frac{\sigma_f B_0^2}{b \rho_f}, \gamma = \frac{\lambda_2 b}{1 - \alpha t}, \lambda = \beta^2 \tag{15}$$

Physical quantities like the Skin friction coefficient and the local Nusselt number are given as

$$Nu_x = \frac{xq_w(x)}{k_f(T_s - T_0)}, C_f = \frac{\tau_w}{\rho_f u_w^2}, \tag{16}$$

$$q_w(x) = -k_{nf} \left(\frac{\partial T}{\partial y} \right)_{y=0}, \tau_w = \mu_{nf} \left(\frac{\partial u}{\partial y} \right)_{y=0}$$

Additionally, in dimensionless form, as follows:

$$C_f Re_x^{1/2} = \frac{1}{\beta(1-\phi)^{2.5}} f''(0), \tag{17}$$

$$Nu_x Re_x^{-1/2} = -\frac{1}{\beta} \left(\frac{k_{nf}}{k_f} + \frac{4}{3} R \right) \theta'(0)$$

3. Entropy Generation

The entropy generation under the aforementioned assumptions is given as below:

$$E_{gen}''' = \frac{k_f}{T_0^2} \left[\frac{k_{nf}}{k_f} + \frac{16T_\infty^3 \sigma^*}{3k^* k_f} \right] \left(\frac{\partial T}{\partial y} \right)^2 + \frac{\mu_{nf}}{T_0} \left(\frac{\partial u}{\partial y} \right)^2 + \frac{\sigma_{nf}}{T_0} B^2(t) u^2 \cos^2 \varepsilon \tag{18}$$

where all terms defined in Equation (15) portray the usual meaning. The entropy generation N_G is defined as

$$N_G = \left(\frac{k_{nf}}{k_f} + \frac{4}{3}R \right) Re_x \theta'^2 + \frac{1}{(1-\phi)^{2.5}} \frac{Br Re_x}{\alpha} f''^2 + \frac{BrM}{\alpha} \frac{\sigma_{nf}}{\sigma_f} \cos^2 \varepsilon f'^2 \tag{19}$$

where S_0''' and S_{gen}''' are the characteristic entropy generation rate and the entropy generation rate. The parameters defined in the above equation are given as

$$\alpha = \frac{\Delta T}{T_{w0}}, Br = \frac{\mu_f u_w^2}{k_f \Delta T}, Re_x = \frac{u_w x}{\nu_f} \tag{20}$$

4. Results and Discussion

This section is devoted to witnessing the impression of numerous parameters on the involved profiles whilst keeping in view their physical significance. The MATLAB built-in function `bvp4c` is utilized to address the differential Equations (9), (10), and (16) with the associated boundary conditions of Equation (11). To solve these, first we have converted the 2nd and 3rd order differential equations to the 1st order by introducing new parameters. The tolerance for the existing problem is fixed as 10^{-6} . The initial guess we yield must satisfy the boundary conditions asymptotically and the solution as well. The results show the influence of solid volume fraction (ϕ), dimensionless film thickness (λ), magnetic parameter (M), unsteadiness parameter (S), radiation parameter (R), thermal relaxation parameter (γ), and non-uniform heat source/sink parameter on the velocity, temperature and entropy generation profiles. Further, the numerical values for the Skin friction and Nusselt number are given in Tables 3 and 4 for different parameters. The numerical values of the parameters are fixed as $\phi = 0.1, A^* = B^* = \lambda = \gamma = 0.5 = S, R = 1.0 = M,$ and $P_r = 6.2$. Figures 2 and 3 display the impact of solid volume fraction (ϕ) on axial velocity and temperature distribution. For incremented values of the solid volume fraction (ϕ), the velocity and temperature profiles enhance in case of both SWCNTs and MWCNTs. Actually, the convective flow and the solid volume fraction are directly proportionate with each other and this is the main reason behind the enhancement of axial velocity and the temperature of the fluid.

Table 3. The comparison table of $-\theta'(0)$ with Sandeep [17] for varied estimates of S when $R = M = \gamma = 0, P_r = 1.0$.

S	$\phi = 0$	
	Sandeep [17]	Present Result
1.0	2.6772221621	2.677222
1.2	1.9995914260	1.999591
1.4	1.4477543611	1.447754
1.6	0.9566978443	0.956697
1.8	0.4845366320	0.484536

Table 4. The numerical value of the Skin friction with $P_r = 6.2$.

ϕ	S	λ	M	$-C_f Re_x^{\frac{1}{2}}$	
–	–	–	–	SWCNTs	MWCNTs
0.1	0.1	0.1	1.0	0.53775	0.52995
0.2	–	–	–	0.57083	0.55402
0.3	–	–	–	0.60395	0.57701
–	0.1	–	–	0.53775	0.52995
–	0.2	–	–	0.54610	0.53761
–	0.3	–	–	0.55442	0.54524
–	–	0.1	–	0.53775	0.52995
–	–	0.2	–	0.62530	0.61054
–	–	0.3	–	0.70792	0.68693
–	–	–	0.0	0.12194	0.11183
–	–	–	0.5	0.34094	0.33214
–	–	–	1.0	0.53775	0.52995

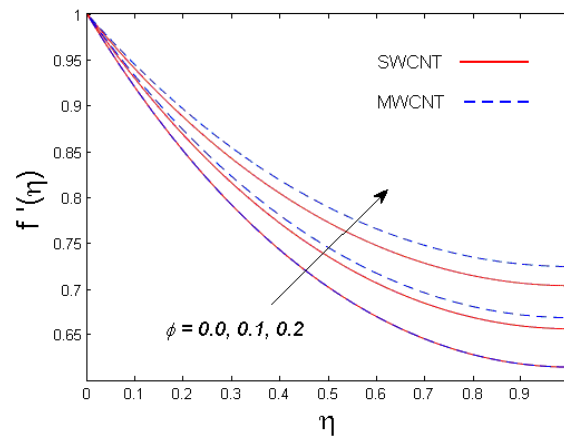


Figure 2. The illustration of ϕ versus $f'(\eta)$.

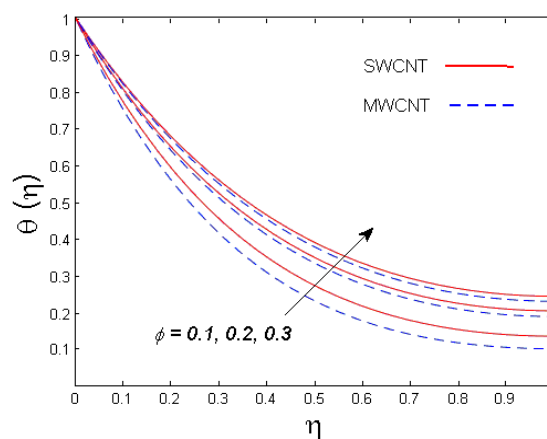


Figure 3. The illustration of ϕ versus $\theta(\eta)$.

Figures 4 and 5 depict the behavior of axial velocity and the temperature field for the growth estimates of the film thickness parameter λ . It is found that both velocity and temperature profiles diminish for increasing values of the film thickness parameter λ . In fact, the more the film thickness, the lesser the fluid motion. This is because of the fact that higher values of film thickness dominate the viscous forces, eventually diminishing the fluid velocity. Similar behavior is observed for the temperature field.

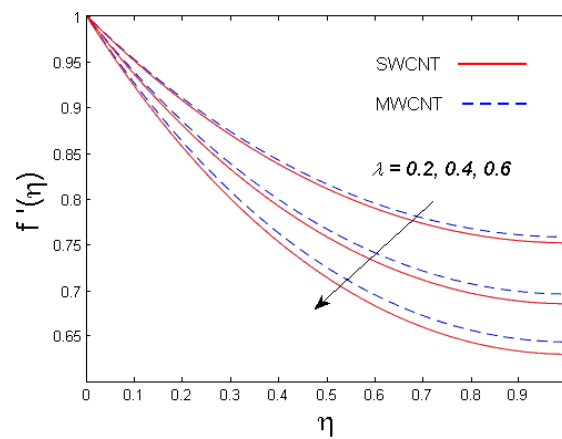


Figure 4. The illustration t of λ versus $f'(\eta)$.

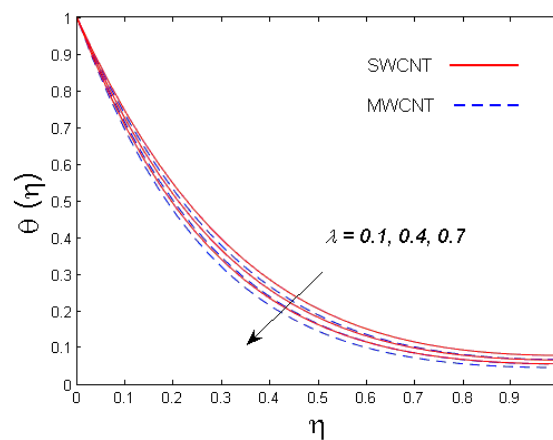


Figure 5. The illustration t of λ versus $\theta(\eta)$.

The effect of the magnetic parameter M on the velocity and temperature fields can be visualized in Figures 6 and 7. Figure 6 displays the impact of the magnetic parameter M on axial velocity. The is the axial velocity of the declining function of the magnetic parameter M . Physically, by enhancing the magnetic parameter M , the Lorentz force is strengthened in the flow, which has a tendency to resist the fluid's motion and slow it down. This force also creates heat energy in the flow. Consequently, the temperature distribution increases both the SWCNTs and MWCNTs, which is displayed in Figure 7.

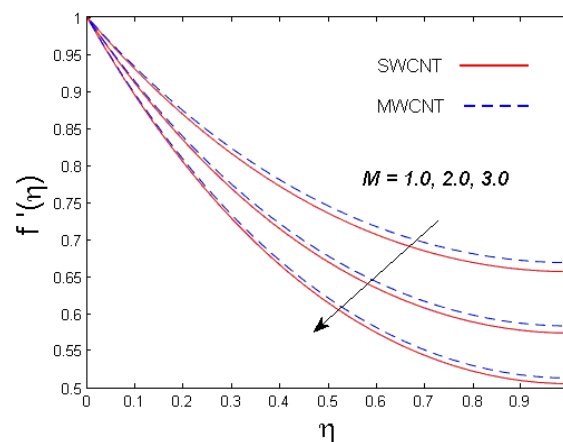


Figure 6. The illustration of M versus $f'(\eta)$.

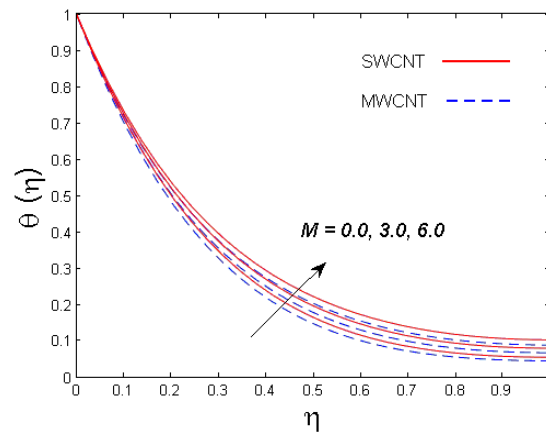


Figure 7. The illustration of M versus $\theta(\eta)$.

Figures 8 and 9 show the effect of the unsteadiness parameter S on the velocity and temperature distributions. It is found that with the increase of the unsteadiness parameter S , the axial velocity diminishes. Physically, the bouncy effect acts on the flow and diminishes it due to the increase in the unsteadiness parameter S . Therefore, the thermal and momentum boundary layer thicknesses decrease.

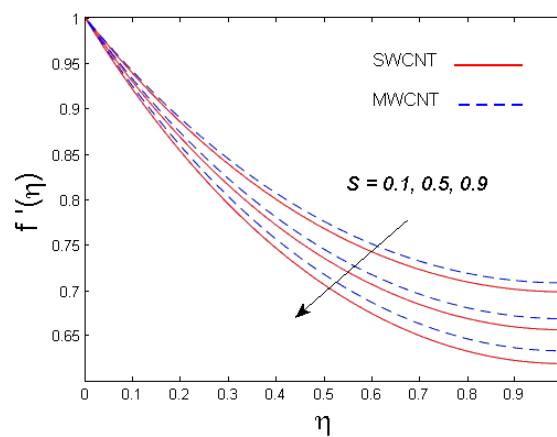


Figure 8. The illustration of S versus $f'(\eta)$.

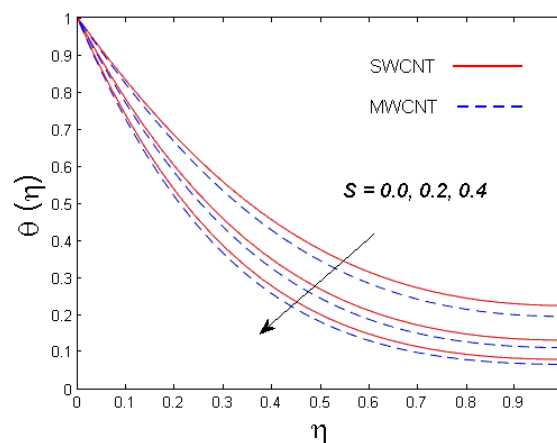


Figure 9. The illustration of S versus $\theta(\eta)$.

Figure 10 determines the consequence of the thermal relaxation parameter γ on the temperature of the fluid. It is concluded that the temperature diminishes for increased values of the thermal relaxation parameter γ . The temperature tends to be sharper near the boundary as the value of γ is higher than the points on the growth in the wall slope of the temperature profile.

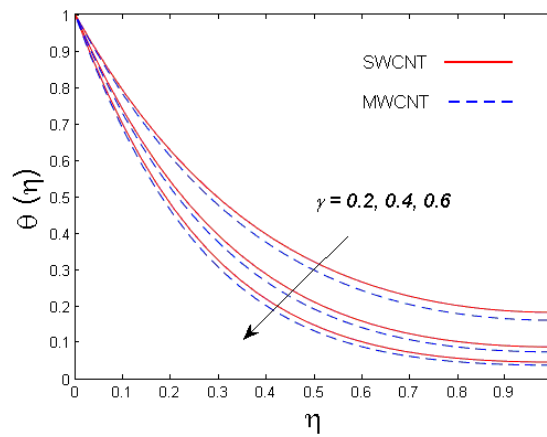


Figure 10. The illustration of γ versus $\theta(\eta)$.

Figure 11 demonstrates the impact of the radiation parameter R on the temperature profile. It is comprehended that the temperature field is an increasing function of the radiation parameter R . It is also concluded that the thermal boundary layer thickness for both carbon nanotubes is increased. In fact, larger estimates of the radiation parameter reduce the mean absorption coefficient and enhance the radiative heat flux's divergence. Due to this, the temperature of the fluid is upsurged.

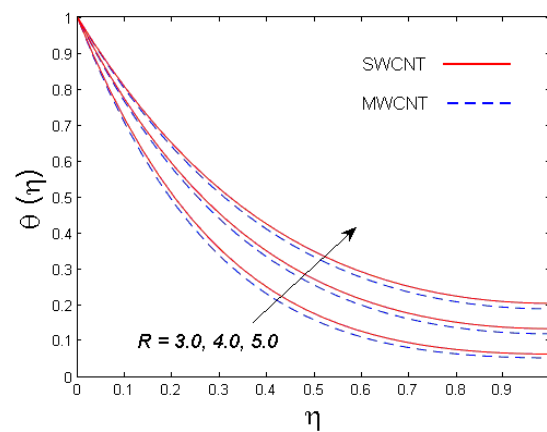


Figure 11. The illustration of R versus $\theta(\eta)$.

The influence of non-uniform heat source/sink parameters A^* and B^* on the temperature distribution is shown in Figures 12 and 13. It can be understood that the temperature profile augments the boosted estimates of non-uniform heat source/sink parameters.

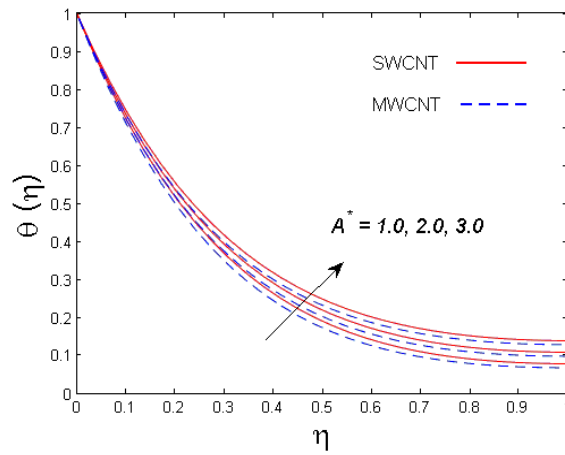


Figure 12. The illustration of A^* versus $\theta(\eta)$.

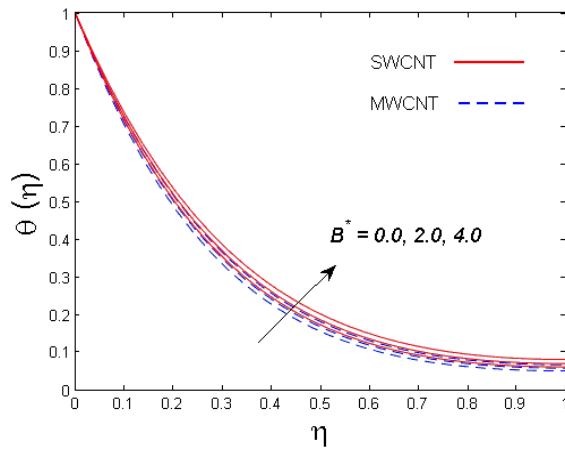


Figure 13. The illustration of B^* versus $\theta(\eta)$.

The effect of Brinkman number (B_r), magnetic parameter (M) and Reynolds number (Re_x) on the averaged entropy generation number is demonstrated in Figures 14–16. It is concluded that the entropy generation number increases for mounting estimations of Brinkman number (B_r), magnetic parameter (M) and Reynolds number (Re_x) for both SWCNT and MWCNT.

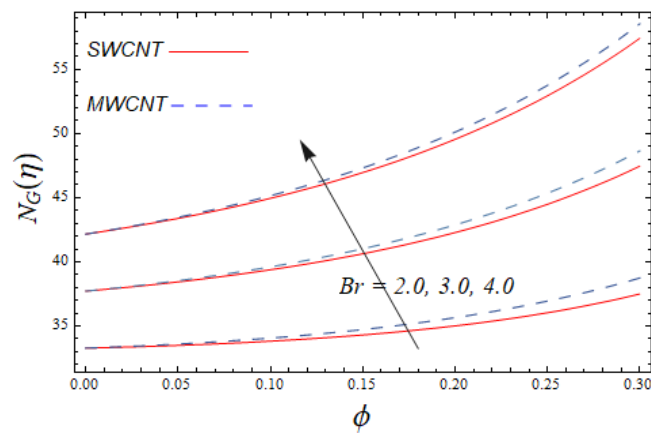


Figure 14. The illustration of B_r versus $N_G(\eta)$.

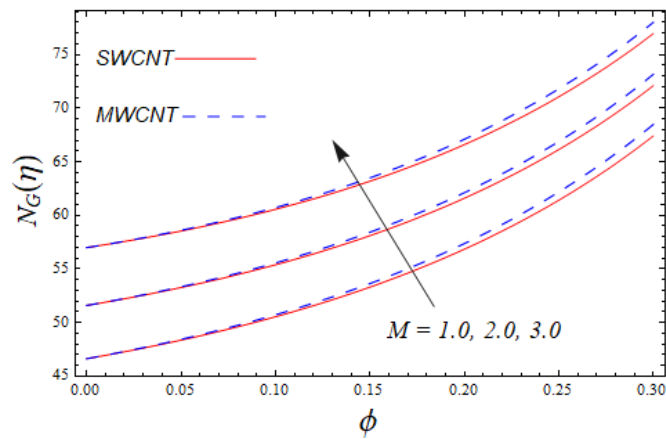


Figure 15. The illustration of M versus $N_G(\eta)$.

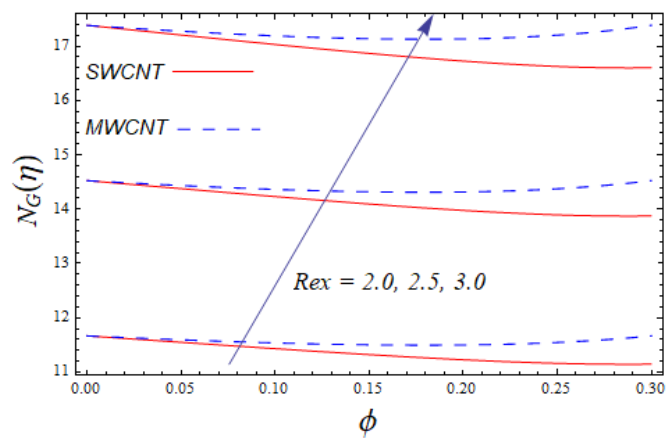


Figure 16. The illustration of Re_x versus $N_G(\eta)$.

Table 3 is erected to envision the precision of the presented model by comparing it with Sandeep [17] who discusses the flow of nanofluids past a thin film under the influence of the magnetic field. To make a comparison, we have neglected the impacts of the volume fraction, electrical conductivity, and thermal relaxation parameters. Excellent alignment is achieved between both results.

Table 4 shows the estimates of the Skin friction coefficient for different parameters. It is seen that the Skin friction coefficient increases for growing values of the magnetic parameter, solid volume fraction, unsteadiness parameter, and film thickness. Table 5 demonstrates the numerical values of Nusselt number for numerous parameters. It is determined that the Nusselt number increases with augmented values of the dimensionless film thickness, radiation parameter, solid volume fraction, and unsteadiness parameter, while it diminishes for growing values of non-uniform heat source/sink.

Table 5. The numerical value of the Nusselt number with $\gamma = 0.1$, $P_r = 6.2$.

Λ	R	ϕ	A^*	B^*	S	$Nu_x Re_x^{-\frac{1}{2}}$	
–	–	–	–	–	–	SWCNTs	MWCNTs
0.1	0.1	0.1	0.1	0.1	0.1	2.11090	2.06990
0.2	–	–	–	–	–	3.27730	3.16440
0.3	–	–	–	–	–	4.46510	4.24750
–	0.1	–	–	–	–	2.36350	2.06990
–	0.3	–	–	–	–	2.36770	2.07060
–	0.5	–	–	–	–	2.37230	2.07130
–	–	0.1	–	–	–	2.11090	2.06990
–	–	0.2	–	–	–	2.59370	2.54840
–	–	0.3	–	–	–	2.84440	2.84000
–	–	–	0.1	–	–	2.11800	2.06990
–	–	–	0.3	–	–	1.93540	1.89220
–	–	–	0.5	–	–	1.75270	1.71440
–	–	–	–	0.1	–	2.11800	2.06990
–	–	–	–	0.3	–	1.88910	1.85770
–	–	–	–	0.5	–	1.66430	1.25340
–	–	–	–	–	0.1	2.11090	2.06990
–	–	–	–	–	0.2	2.81360	2.72250
–	–	–	–	–	0.3	3.66060	3.48490

5. Conclusions

The thin film flow of nanofluid comprising of CNTs of both types (SWCNTs/MWCNTs) is studied whilst keeping in view the important applications of CNTs in many engineering applications. The flow is supported by the additional effects like C-C heat flux and entropy generation. The model is solved numerically with the support of the MATLAB software function bvp4c. The highlights of the existing study are

- Velocity and temperature distributions are mounting functions of the solid volume fraction for both types of CNTs in case of the thin film flow.
- For growing estimates of the thin film thickness parameter, the axial velocity diminishes.
- The velocity and temperature distributions show an opposite trend for the strong magnetic field in a thin film flow model.
- Larger estimates of heat source/sink parameter lead to an increase in the temperature of the fluid.
- The temperature of the fluid is decreased for higher values of the thermal relaxation parameter.
- With an increase in the estimates of film thickness, the magnetic parameter and the Skin friction coefficient show mounting behavior.
- The Nusselt number shows declining behavior for growing values of non-uniform heat source/sink.
- Entropy generation in the case of thin film flow is higher for larger estimates of the Brinkman number and the magnetic parameter.

Author Contributions: Data Curation, D.L.; Funding Acquisition, F.H.; Investigation, M.M.; Project Administration, M.R.; F.H.; Resources, D.L.; Software, M.M.; Supervision, M.M.; Validation, F.H.; Visualization, J.D.C.; Writing—Original Draft, J.D.C.

Funding: This research was funded by Zayed University research fund, Abu Dhabi, UAE.

Conflicts of Interest: The authors declare no conflict of interest.

Nomenclature

u, v	velocity components	B_0	magnetic field of strength
x, y	coordinate axis	P_r	Prandtl number
ξ	stream function	C_f	skin friction coefficient
B	magnetic field	Nu_x	Nusselt number
T_w	constant surface temperature	S	squeezing parameter
T	temperature	α	thermal diffusivity
Ω_2	Cattaneo–Christov parameter	Re_x	local reynolds number
q	heat source/sink	S_0	characteristic entropy generation
C_p	specific heat	S_{gen}	entropy generation rate
ρ	density	k_0	thermal conductivity near from the surface
λ_2	relaxation time of the heat flux	k_f	thermal conductivity of water
T_∞	ambient fluid temperature	ε	thermal conductivity parameter
u_w	stretching velocity along x -direction	N_G	entropy generation number

Greek Symbols

ρ_{CNT}, ρ_f	density of nanofluid	f	dimensionless stream function
σ^*	Stephan-Boltzmann constant	θ	dimensionless temperature
μ_{nf}, μ_f	dynamic viscosity	γ	thermal relaxation parameter
k^*	viscoelastic parameter	λ	relaxation time of heat flux
α_{nf}	modified thermal diffusivity	σ_{nf}, σ_f	electrical conductivity of nanofluid and base fluid
$(\rho C_p)_{nf}, (\rho C_p)_f$	heat capacity	ν_{nf}, ν_f	kinematic viscosity of nanofluid
k, k_{nf}	thermal conductivity	ΔT	temperature difference
φ	solid volume fraction of nanofluid	τ_w	shear stress
η	a scaled boundary-layer coordinate	T_w	temperature on the interface
Ψ	stream function	B_r	brinkmann number
$q_w(x)$	the surface heat flux of nanoliquid film	M	hartmann number
β	thermal expansion coefficient	R	conduction radiation parameter
A^*, B^*	non-uniform heat source/sink parameters		

References

1. Aziz, R.C.; Hashim, I.; Alomari, A.K. Thin film flow and heat transfer on an unsteady stretching sheet with internal heating. *Meccanica* **2011**, *46*, 349–357. [[CrossRef](#)]
2. Wang, C.Y. Liquid film on an unsteady stretching surface. *Q. Appl. Math.* **1990**, *48*, 601–610. [[CrossRef](#)]
3. Andersson, H.I.; Aarseth, J.B.; Dandapat, B.S. Heat transfer in a liquid film on an unsteady stretching surface. *Int. J. Heat Mass Transf.* **2000**, *43*, 69–74. [[CrossRef](#)]
4. Liu, I.C.; Andersson, H.I. Heat transfer in a liquid film on an unsteady stretching sheet. *Int. J. Therm. Sci.* **2008**, *47*, 766–772. [[CrossRef](#)]
5. Wang, C. Analytic solutions for a liquid film on an unsteady stretching surface. *Heat Mass Transf.* **2006**, *42*, 759–766. [[CrossRef](#)]
6. Abel, M.S.; Mahesha, N.; Tawade, J. Heat transfer in a liquid film over an unsteady stretching surface with viscous dissipation in presence of external magnetic field. *Appl. Math. Model.* **2009**, *33*, 3430–3441. [[CrossRef](#)]
7. Noor, N.F.M.; Abdulaziz, O.; Hashim, I. MHD flow and heat transfer in a thin liquid film on an unsteady stretching sheet by the homotopy analysis method. *Int. J. Numer. Methods Fluids* **2010**, *63*, 357–373. [[CrossRef](#)]
8. Dandapat, B.S.; Santra, B.; Andersson, H.I. Thermocapillarity in a liquid film on an unsteady stretching surface. *Int. J. Heat Mass Transf.* **2003**, *46*, 3009–3015. [[CrossRef](#)]
9. Wang, C.; Pop, I. Analysis of the flow of a power-law fluid film on an unsteady stretching surface by means of homotopy analysis method. *J. Non-Newton. Fluid Mech.* **2006**, *138*, 161–172. [[CrossRef](#)]
10. Chen, C.H. Effect of viscous dissipation on heat transfer in a non-Newtonian liquid film over an unsteady stretching sheet. *J. Non-Newton. Fluid Mech.* **2006**, *135*, 128–135. [[CrossRef](#)]
11. Chen, C.H. Marangoni effects on forced convection of power-law liquids in a thin film over a stretching surface. *Phys. Lett. A* **2007**, *370*, 51–57. [[CrossRef](#)]
12. Abbas, Z.; Hayat, T.; Sajid, M.; Asghar, S. Unsteady flow of a second-grade fluid film over an unsteady stretching sheet. *Math. Comput. Model.* **2008**, *48*, 518–526. [[CrossRef](#)]
13. Choi, S.U.; Eastman, J.A. *Enhancing Thermal Conductivity of Fluids with Nanoparticles*; No. ANL/MSD/CP-84938; CONF-951135-29; Argonne National Lab.: DuPage County, IL, USA, 1995.

14. Sheikholeslami, M.; Ganji, D.D. Nanofluid flow and heat transfer between parallel plates considering Brownian motion using DTM. *Comput. Methods Appl. Mech. Eng.* **2015**, *283*, 651–663. [[CrossRef](#)]
15. Lin, Y.; Zheng, L.; Zhang, X.; Ma, L.; Chen, G. MHD pseudo-plastic nanofluid unsteady flow and heat transfer in a finite thin film over stretching surface with internal heat generation. *Int. J. Heat Mass Transf.* **2015**, *84*, 903–911. [[CrossRef](#)]
16. Lin, Y.; Zheng, L.; Chen, G. Unsteady flow and heat transfer of pseudo-plastic nanofluid in a finite thin film on a stretching surface with variable thermal conductivity and viscous dissipation. *Powder Technol.* **2015**, *274*, 324–332. [[CrossRef](#)]
17. Sandeep, N. Effect of aligned magnetic field on liquid thin film flow of magnetic-nanofluids embedded with graphene nanoparticles. *Adv. Powder Technol.* **2017**, *28*, 865–875. [[CrossRef](#)]
18. Zhang, Y.; Zhang, M.; Bai, Y. Flow and heat transfer of an Oldroyd-B nanofluid thin film over an unsteady stretching sheet. *J. Mol. Liq.* **2016**, *220*, 665–670. [[CrossRef](#)]
19. Zhang, Y.; Zhang, M.; Bai, Y. Unsteady flow and heat transfer of power-law nanofluid thin film over a stretching sheet with variable magnetic field and power-law velocity slip effect. *J. Taiwan Inst. Chem. Eng.* **2017**, *70*, 104–110. [[CrossRef](#)]
20. Fakour, M.; Rahbari, A.; Khodabandeh, E.; Ganji, D.D. Nanofluid thin film flow and heat transfer over an unsteady stretching elastic sheet by LSM. *J. Mech. Sci. Technol.* **2018**, *32*, 177–183. [[CrossRef](#)]
21. Ishaq, M.; Ali, G.; Shah, Z.; Islam, S.; Muhammad, S. Entropy generation on nanofluid thin film flow of Eyring–Powell fluid with thermal radiation and MHD effect on an unsteady porous stretching sheet. *Entropy* **2018**, *20*, 412. [[CrossRef](#)]
22. Nasir, S.; Shah, Z.; Islam, S.; Bonyah, E.; Gul, T. Darcy Forchheimer nanofluid thin film flow of SWCNTs and heat transfer analysis over an unsteady stretching sheet. *AIP Adv.* **2019**, *9*, 015223. [[CrossRef](#)]
23. Pal, D.; Chatterjee, S. Soret and Dufour effects on MHD convective heat and mass transfer of a power-law fluid over an inclined plate with variable thermal conductivity in a porous medium. *Appl. Math. Comput.* **2013**, *219*, 7556–7574. [[CrossRef](#)]
24. Vajravelu, K.; Prasad, K.V.; Ng, C.O. Unsteady convective boundary layer flow of a viscous fluid at a vertical surface with variable fluid properties. *Nonlinear Anal. Real World Appl.* **2013**, *14*, 455–464. [[CrossRef](#)]
25. Cattaneo, C. Sulla conduzione del calore. *Atti Sem. Mat. Fis. Univ. Modena* **1948**, *3*, 83–101.
26. Tibullo, V.; Zampoli, V. A uniqueness result for the Cattaneo-Christov heat conduction model applied to incompressible fluids. *Mech. Res. Commun.* **2011**, *38*, 77–79. [[CrossRef](#)]
27. Han, S.; Zheng, L.; Li, C.; Zhang, X. Coupled flow and heat transfer in viscoelastic fluid with Cattaneo-Christov heat flux model. *Appl. Math. Lett.* **2014**, *38*, 87–93. [[CrossRef](#)]
28. Mustafa, M. Cattaneo-Christov heat flux model for rotating flow and heat transfer of upper-convected Maxwell fluid. *AIP Adv.* **2015**, *5*, 047109. [[CrossRef](#)]
29. Khan, J.A.; Mustafa, M.; Hayat, T.; Alsaedi, A. Numerical study of Cattaneo-Christov heat flux model for viscoelastic flow due to an exponentially stretching surface. *PLoS ONE* **2015**, *10*, e0137363.
30. Lu, D.; Li, Z.; Ramzan, M.; Shafee, A.; Chung, J.D. Unsteady squeezing carbon nanotubes based nano-liquid flow with Cattaneo-Christov heat flux and homogeneous–heterogeneous reactions. *Appl. Nanosci.* **2019**, *9*, 169–178. [[CrossRef](#)]
31. Ramzan, M.; Bilal, M.; Chung, J.D. MHD stagnation point Cattaneo-Christov heat flux in Williamson fluid flow with homogeneous–heterogeneous reactions and convective boundary condition—A numerical approach. *J. Mol. Liq.* **2017**, *225*, 856–862. [[CrossRef](#)]
32. Alamri, S.Z.; Khan, A.A.; Azeez, M.; Ellahi, R. Effects of mass transfer on MHD second grade fluid towards stretching cylinder: A novel perspective of Cattaneo-Christov heat flux model. *Phys. Lett. A* **2019**, *383*, 276–281. [[CrossRef](#)]
33. Ramzan, M.; Bilal, M.; Chung, J.D. Influence of homogeneous-heterogeneous reactions on MHD 3D Maxwell fluid flow with Cattaneo-Christov heat flux and convective boundary condition. *J. Mol. Liq.* **2017**, *230*, 415–422. [[CrossRef](#)]
34. Ramzan, M.; Bilal, M.; Chung, J.D. Effects of MHD homogeneous-heterogeneous reactions on third grade fluid flow with Cattaneo-Christov heat flux. *J. Mol. Liq.* **2016**, *223*, 1284–1290. [[CrossRef](#)]
35. Alshomrani, A.S.; Ullah, M.Z. Effects of homogeneous–heterogeneous reactions and convective condition in Darcy–Forchheimer flow of carbon nanotubes. *J. Heat Transf.* **2019**, *141*, 012405. [[CrossRef](#)]

36. Nasir, S.; Shah, Z.; Islam, S.; Khan, W.; Bonyah, E.; Ayaz, M.; Khan, A. Three dimensional Darcy-Forchheimer radiated flow of single and multiwall carbon nanotubes over a rotating stretchable disk with convective heat generation and absorption. *AIP Adv.* **2019**, *9*, 035031. [[CrossRef](#)]
37. Shah, Z.; Tassaddiq, A.; Islam, S.; Alklaibi, A.M.; Khan, I. Cattaneo-Christov heat flux model for three-dimensional rotating flow of SWCNT and MWCNT nanofluid with Darcy–Forchheimer porous medium induced by a linearly stretchable surface. *Symmetry* **2019**, *11*, 331. [[CrossRef](#)]
38. Gul, T.; Khan, M.A.; Noman, W.; Khan, I.; Abdullah Alkanhal, T.; Tlili, I. Fractional order forced convection carbon nanotube nanofluid flow passing over a thin needle. *Symmetry* **2019**, *11*, 312. [[CrossRef](#)]
39. Khan, A.S.; Nie, Y.; Shah, Z. Impact of thermal radiation and heat source/sink on MHD time-dependent thin-film flow of Oldroyed-B, Maxwell, and Jeffery fluids over a stretching surface. *Processes* **2019**, *7*, 191. [[CrossRef](#)]
40. Jinkins, K.R.; Chan, J.; Jacobberger, R.M.; Berson, A.; Arnold, M.S. Substrate-wide confined shear alignment of carbon nanotubes for thin film transistors. *Adv. Electron. Mater.* **2019**, *5*, 1800593. [[CrossRef](#)]
41. Narayana, M.; Sibanda, P. Laminar flow of a nanoliquid film over an unsteady stretching sheet. *Int. J. Heat Mass Transf.* **2012**, *55*, 7552–7560. [[CrossRef](#)]
42. Xu, H.; Pop, I.; You, X.C. Flow and heat transfer in a nano-liquid film over an unsteady stretching surface. *Int. J. Heat Mass Transf.* **2013**, *60*, 646–652. [[CrossRef](#)]
43. Qasim, M.; Khan, Z.H.; Lopez, R.J.; Khan, W.A. Heat and mass transfer in nanofluid thin film over an unsteady stretching sheet using Buongiorno’s model. *Eur. Phys. J. Plus* **2016**, *131*, 16. [[CrossRef](#)]



© 2019 by the authors. Licensee MDPI, Basel, Switzerland. This article is an open access article distributed under the terms and conditions of the Creative Commons Attribution (CC BY) license (<http://creativecommons.org/licenses/by/4.0/>).